Verification and Validation standards on Rotor Dynamics analysis software

Edgard Haenisch Porto[1], Diogo Stuani Alves[2] and Katia Lucchesi Cavalca [1]

[1] Universidade Estadual de Campinas (Unicamp), Faculdade de Engenharia Mecânica (FEM). Mendeleyev Street, 200, 13083860 – Campinas, SP – Brazil. Phone: +55 (19) 35213178

[2] Department of Mechanical Engineering, University of Bath, BA2 7 AY, Bath, UK.

Abstract:

Assessments of verification, validation and quantification of uncertainties are being increasingly used to certify that softwares are free of errors. The benefits imply greater relevance of the assessed softwares in the market and experimental tests can be dispensed from future projects, decreasing lead time for launching a product while keeping its reliability. This work focuses on a Rotor Dynamics software verification, validation, and uncertainty quantification, regarding the ASME V&V 10, 10.1, and 20. Since the ASME V&V 10 and 10.1 standards deal with the verification, validation and quantification of uncertainties in the field of solid mechanics, they will be used to evaluate the rotor shaft discretization. On the other hand, the ASME V&V 20 standard is related to fluid mechanics; therefore, it will be used to assess the discretization of the oil film mesh, present in the fluid film bearings. Firstly, the analytic and numeric models are briefly presented. Both are respectively used in the verification and validation assessments. The verification assessment is divided in three parts: the rotor static and dynamic behavior (without hydrodynamic bearings); the hydrodynamic bearings themselves; and the static and dynamic behavior of the rotor supported by hydrodynamic bearings. Then, the validation assessment is achieved using a set of experimental data, which contains unbalance response functions (URF) at bearings and disk positions. Finally, the conclusions and remarks are presented.

Keywords: ASME, Verification and validation, bearings, rotors.

INTRODUCTION

The history of the Verification and Validation (V&V) standards begins in 2006 when the first AMSE V&V standard was released (ASME, 2006) addressing computational solid mechanics. However, previous efforts which would culminate in the aforementioned standard were also being made. At first, the Institute of Electrical and Electronic Engineers (IEEE) was in charge to adopt guidelines and standards for Software Quality Assurance (SQA). In 1993, the "Guide to the Expression of Uncertainty in Measurement" was published by the International Organization for Standardization (ISO) and other six organizations (ASME, 2009). The American Institute of Aeronautics and Astronautics (AIAA) created the "Guide for Verification and Validation of Computational Fluid Dynamics Simulations" in 1998 (ASME, 2006).

According to Hu et al, (2016), workshops sponsored by Sandia National Laboratories about uncertainty started in 2002. As presented by Hills et al. (2008), another workshop about V&V problems organized by Sandia happened in the same year as the first ASME V&V standard, addressing the Verification and Validation in Computational Solid Mechanics. Some of these workshops introduced challenging problems to participants (mostly engineers and mathematicians), which were useful to create discussions, and improve and detail future guidelines. Other workshops were focused on theories and methodologies instead. Both ways tried to overcome the difficulty of establishing quantitative parameters according to qualitative ones mutually. However, this is not an excuse to not release standards with the current available knowledge.

Parallel to workshops organizations, other standards were released. The ASME V&V 20 (AMSE, 2009), covering Computational Fluid Dynamics and Heat Transfer, bases itself on the AIAA standard. In 2012, a new edition of the V&V 10 including an illustrative example of how the standard could be applied to cantilever beam was released (ASME, 2012). Afterwards other V&V guides for other fields have been created, for example one regarding the evaluation of the predictive capability of the Virtual Environment software for reactor applications (Athe, Jones, and Dinh, 2021), and other regarding standardized in silico clinical trial procedures, aiming to reduce medical device testing costs (Bodner and Kaul, 2021).

Thus, the objective of this work is to perform the verification and validation assessments on a software that makes analysis of rotors modeled by the Finite Element Methods (FEM). The number of System Response Quantities (SRQs) available for the verification stage is greater than the number of SRQs available for the validation stage. Meanwhile, the SRQs analyzed in the validation assessment are results of other implicit SRQs, making this a brief, but also effective, study.

MODELING

The verification assessment is divided in code verification and calculation verification. The code verification requires both analytic and numerical modeling, while the calculation verification requires just the numerical modeling. The validation assessment also requires the numerical modeling, but alongside experimental results.

Analytic modeling

The analytic modeling for statical and dynamic behaviors is based, respectively, on the beam theory deflection and Laval rotor.

Static behavior modeling

The beam modeling, found in several solid mechanics references, such as Hibbeler (2010), is based on the Bernoulli-Euler beam theory, which considers that the transversal sections are perpendicular to the deflection line. Eq. 1 summarizes the beam behavior, where E is the Young's modulus; I is the second moment of area for the beam's transversal section; x is the variable describing the beam length; $w(x)$ is the distributed load function; $V(x)$ is the shear force; $M(x)$ is the bending moment; $\theta(x)$ is the angle of rotation and $\xi(x)$ is the deflection (or vertical displacement).

$$EI\frac{d^4}{dx^4}\xi(x) = EI\frac{d^3}{dx^3}\theta(x) = \frac{d^2}{dx^2}M(x) = \frac{d}{dx}V(x) = w(x) \tag{1}$$

Hibbeler (2010) also mentions the singularity function, showed on Eq. 2, that can be added to the load function $w(x)$ multiplied to moments, concentrated forces or distributed loads in certain parts of the beam. The number n is an exponential associated with the kind of load added on the load function $w(x)$, the exponent $n = -2$ is associated with bending moments, $n = -1$ is associated with shear forces and $n = 0$ is associated with distributed loads.

$$\langle x-a\rangle^n = \begin{cases} 0, & for \;\; x < a \;\; or \;\; n < 0 \\ (x-a)^n, & for \;\; x \geq a \;\; and \;\; n \geq 0 \end{cases} \tag{2}$$

The calculations concerning the analytic model begin with the integration of the load function $w(x)$. If the resulting exponent from the integration of the singularity function is lower than zero, than this function will not be multiplied by any terms. Instead, the exponent will just rise by one unit. Once the resulting exponent value is zero, the integration will proceed as given by the traditional calculus laws, as shown on Eq. 3. With these information and boundary conditions available, the rotation and deflection functions can be obtained.

$$\int\langle x-a\rangle^n dx = \frac{1}{n+1}\langle x-a\rangle^{n+1}, \;\; for \;\; n \geq 0 \tag{3}$$

Dynamic behavior modeling

Eq. 4 describes the frequency response of a Laval rotor, modeled by Krämer (1993), considering a sinusoidal solution, according to the rotation speed Ω. The matrix $[M]$ is the inertia matrix, $[G]$ is the gyroscopic matrix, $[C] = \beta[K]$ is the proportional damping matrix, $[K]$ is the stiffness matrix, $\{v\}$ is the displacement vector, and $\{F\}$ is the generalized forces vector, in which the unbalance forces can be added.

$$\{-\Omega^2[M] + i\Omega([G] + [C]) + [K]\}\{v\} = \{F\} \tag{4}$$

If just the displacements of the disk are considered (i.e., no displacements at the bearings locations), there are only four degrees of freedom (DOF): horizontal and vertical translations and rotations of the disk; if there are displacements at the bearing regions, four DOF are added: horizontal and vertical translations for both bearings, that is, eight DOF in total.

Krämer (1993) also modeled fluid film bearings using the infinitely short bearing theory in order to define the dynamic coefficients resulted from the oil film forces (damping and stiffness forces) depending on the rotating speed Ω. The modeling starts defining the oil lift force F_η, modified Sommerfeld number S^* (which is the relation between the weight force of rotor applied to the beam F_0 and the oil film lift force F_η), attitude angle φ and oil thickness h, respectively shown on Eqs. 5, 6, 7 and 8. Describing the values and variables, η is the oil dynamic viscosity; R is the internal bearing radius; L is the bearing length; δ is the bearing clearance; the adimensional eccentricity is the absolute eccentricity e divided by clearance ($\varepsilon = e/\delta$); and the bearing circumferential coordinate is θ. The definition of the attitude angle is useful to plot the bearing locus.

$$F_\eta = \frac{\eta\Omega R L^3}{\delta^2} \tag{5}$$

$$S^* = \frac{F_0}{F_\eta} = \frac{\pi}{2}\frac{\varepsilon}{(1-\varepsilon^2)^2}\sqrt{1-\varepsilon^2+\left(\frac{4}{\pi}\varepsilon\right)^2} \tag{6}$$

$$\varphi = arctan\left(\frac{\pi}{4}\frac{\sqrt{1-\varepsilon^2}}{\varepsilon}\right) \tag{7}$$

$$h = \delta(1 + \varepsilon.cos\theta) \tag{8}$$

With those definitions, the oil pressure field can be defined using the Reynolds Equation, showed on Eq. 9. The transient portion of the equation takes into account the derivative of the oil film thickness with respect to time t, $x_1 = R\theta$ refers to the circumferential length of the bearing, x_2 refers to the bearing axial length, which is the same direction as the rotor axial direction ($x_2 = x$) and $U = 2\pi R\Omega$ is the circular flow speed on the bearing.

$$\frac{\partial}{\partial x_1}\left(h^3\frac{\partial P}{\partial x_1}\right) + \frac{\partial}{\partial x_2}\left(h^3\frac{\partial P}{\partial x_2}\right) = 6\eta U\frac{\partial h}{\partial x_1} + 12\eta\frac{\partial h}{\partial t} \tag{9}$$

The infinitely short bearing theory neglects the pressure gradient in the circumferential direction (x_1). Also, neglecting the transient effects one has the simplified Reynolds Equation in Eq. 10.

$$h^3\left(\frac{\partial^2 P}{\partial x_1^2}\right) = 6\eta U\frac{\partial h}{\partial \theta}\frac{\partial \theta}{\partial x_1} \tag{10}$$

Finally, the pressure function can be obtained by integrating Eq. 10, resulting in the Eq. 11. By integrating again, one obtains the radial and tangential forces.

$$P(\theta, x) = \frac{3\varepsilon\eta U\, sen\,\theta}{R\delta^2(1+\varepsilon\, cos\,\theta)^3}\left(\frac{L^2}{4} - x^2\right) + P_{atm} \tag{11}$$

Based on the radial and tangential forces, Krämer (1993) defined the stiffness coefficients, shown on Eq. 12 and damping coefficients, shown on Eq. 13.

$$k_{yy} = \gamma_{yy}\frac{F_0}{\delta} \;|\; k_{yz} = \gamma_{yz}\frac{F_0}{\delta} \;|\; k_{zy} = \gamma_{zy}\frac{F_0}{\delta} \;|\; k_{zz} = \gamma_{zz}\frac{F_0}{\delta} \tag{12}$$

$$c_{yy} = \beta_{yy}\frac{F_0}{\delta} \;|\; c_{yz} = \beta_{yz}\frac{F_0}{\delta} \;|\; c_{zy} = \beta_{zy}\frac{F_0}{\delta} \;|\; c_{zz} = \beta_{zz}\frac{F_0}{\delta} \tag{13}$$

Numerical modeling

The numerical model uses the FEM, adopting the rigid disk model by Nelson e McVaugh (1976) and the Timoshenko beam theory (Nelson (1980)) to model several shapes of rotors. The Timoshenko beam considers the shear effect on the beams deformations and is shown on the Fig.1, with coordinates valid for both rigid disk and beam elements.

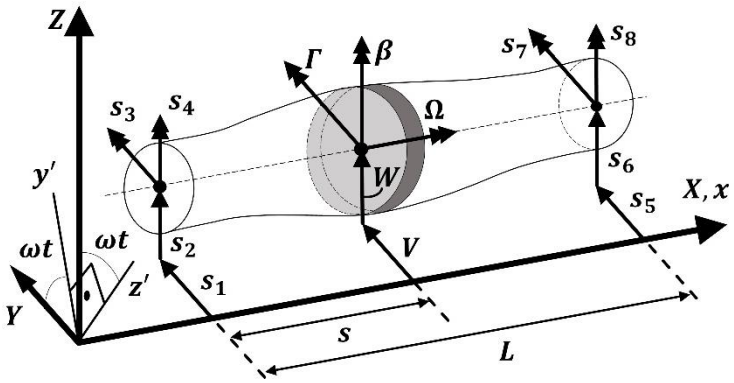

Figure 1 – Beam element model with coordinates.

The bearing damping and stiffness coefficients are again obtained via the complete Reynolds Equation, showed previously on Eq. 9, numerically adapted, which defines the pressure *P* of the oil film by solving system of numerical equations. The pressure field can be numerically integrated by the discretized area, resulting on the hydrodynamic forces, and then, the dynamic coefficients can be calculated for each rotation speed. Since the oil film is very thin, the finite elements are divided only along the circumferential and axial direction.

VERIFICATION AND VALIDATION

In the verification stage, five grids for shaft discretization, as well as five grids for oil film discretization, were chosen. There are five parameters in the verification assessment: one for code verification, which is the observed order of accuracy p_{ve}, and four for calculation verification, which are the theoretical order of accuracy p_{va}, SRQ estimation, error estimation,

and Grid Convergence Index (GCI). For calculation of the observed order of accuracy p_{ve} (from code verification), SRQs resulted from two consecutive grids are required, as shown in Eq. 14, while the other parameters from the calculation verification requires three consecutive grids, so there will be four iterations for code verification and three iterations for calculation verification. The calculated SRQ from the numeric model is SRQ_{nu} ; SRQ_{an} is from the analytic model; el refers to the number of elements from the grid; the index i refers to the most refined grid.

$$p_{ve} = Log\left(\frac{|SRQ_{nu\,i-1} - SRQ_{an}|}{|SRQ_{nu\,i} - SRQ_{an}|}\right) / Log\left(\frac{el_i}{el_{i-1}}\right) \tag{14}$$

The theoretical order of accuracy (from calculation verification) is defined in Eq. 15. h_i is the grid refinement (number of elements), the lower the number i the finer the grid; r is the refinement ratio. For the shaft, the refinement ratio is $r = 2$. The stating number of elements is two: one on the left of the disk and one on the right.

$$p_{va} = Ln\left(\frac{SQR_{nu}(h_3) - SQR_{nu}(h_2)}{SQR_{nu}(h_2) - SQR_{nu}(h_1)}\right) / Ln(r) \tag{15}$$

The estimated SRQ (SQR_{es}) is defined at Eq. 16.

$$SQR_{es} = SQR_{nu}(h_1) \;+\; SQR_{nu}(h_1) - SQR_{nu}(h_2)/(h_2/h_1)^{p_{va}} - 1 \tag{16}$$

The error estimation is defined as the difference between the estimated SQR_{es} and the numeric SRQ from the most refined grid $SQR_{nu}(h_1)$, as shown in Eq. 17:

$$\varepsilon = SQR_{es} - SQR_{nu}(h_1) \tag{17}$$

Finally, the last parameter from the calculation verification is the GCI, defined as $GCI = F_s\varepsilon$ which is the product between a security factor F_s and the error estimation ε. The security factor adopted according to the standard ASME V&V 10.1, for three grids for each iteration is $F_s = 1.25$. When multiplied by the finest numeric SRQ ($SQR_{nu}(h_1)$), an error band is obtained, where the exact solution has a high probability to be. For the oil film grid discretization, the refinement ratio must be less than $r = 2$, due to computational impracticability, but be equal to or greater than $r = 1.3$ according to the standard ASME V&V 20.

Since there are two refinement directions (circumferential and axial), the grid size can be defined as $\zeta = \sqrt{\Delta x \Delta\theta}$ and two refinement ratios are: $r_x = 1.3$ as the ratio related to the bearing length and $r_\theta = 1.6$ as the ratio related to the circumferential direction. The starting number of elements in the axial direction is 21 and in the circumferential direction is 31. The verification parameters definitions for the bearings are omitted. The validation requirement is 10%, while the verification requirement is a percentage (2%) of the validation requirement, which is 0.2%.

The only validation metric is calculated by estimating the Probability Density Functions (PDFs) of the numeric model and experimental results. Afterwards the cumulated Probability Density Functions (CDFs) are calculated. This metric is defined at Eq. 18 where $\overline{SRQ}^{exp}$ is the mean value of the SRQ experimental data, $CDF_{SRQ}num$ is the CDF from the numeric SRQs, $CDF_{SRQ}exp$ from the experimental SRQs and ψ is the physical quantity of the SRQ being assessed.

$$M^{SRQ} = \frac{1}{|\overline{SRQ}^{exp}|}\int_{-\infty}^{\infty}\left|CDF_{SRQ}num(\psi) - CDF_{SRQ}\,exp(\psi)\right| d\psi \tag{18}$$

Rotor parameters

Before the verification or validation assessments be executed, the analytic and numerical models must be adjusted. The analytic models are always the simplest models and can be based on more complex ones, assuming how parameters are going to be simplified. A complete sketch of a rotor with its respective photo in laboratory is shown on Fig 2. The material is steel, with elastic modulus of $E = 200GPa$; density of $\rho = 7850[kg/m^3]$; unbalance mass $m_e = 3g$; eccentricity $e = 40mm$; absolute oil viscosity $\eta = 7 \times 10^{-2}[Pa.s]$; oil film temperature of $T_{oil} = 25$°C; and bearing clearance of $\delta = 90\mu m$.

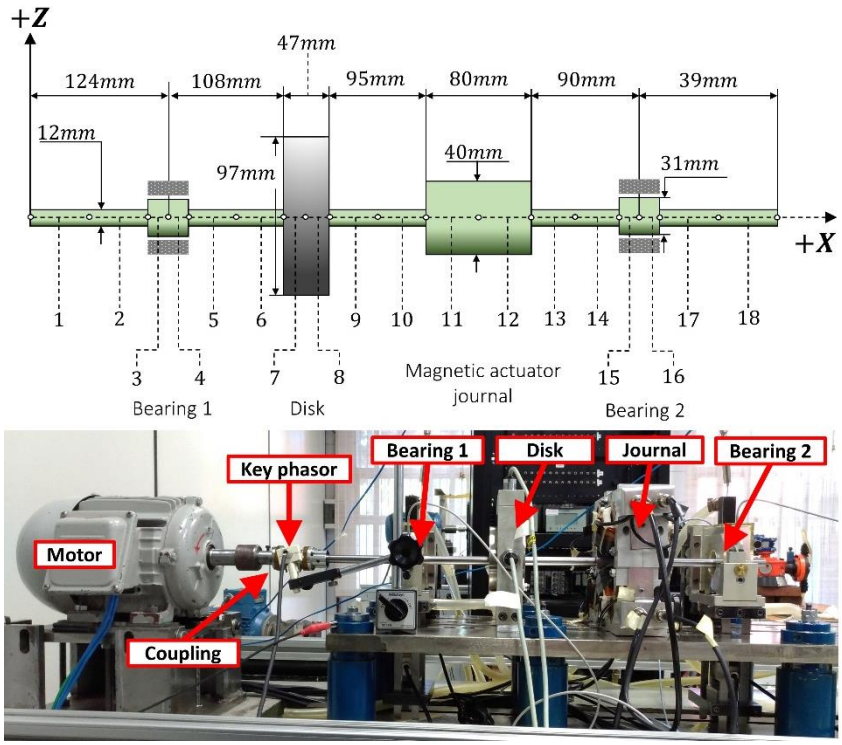

Figure 2 – Rotor sketch (above) and rotor picture (bellow).

As a good engineering practice, both static and dynamic models must have their parameters chosen based on the real-world model. Fig. 3 shows the sketches for static and dynamic models, where both consider the preservation of reaction loads on bearings. One can observe that the statical model considers the distributed load (representing the shaft weight) and the disk weight, while the dynamic model considers only a concentrated load (representing the disk weight, on the disk position).

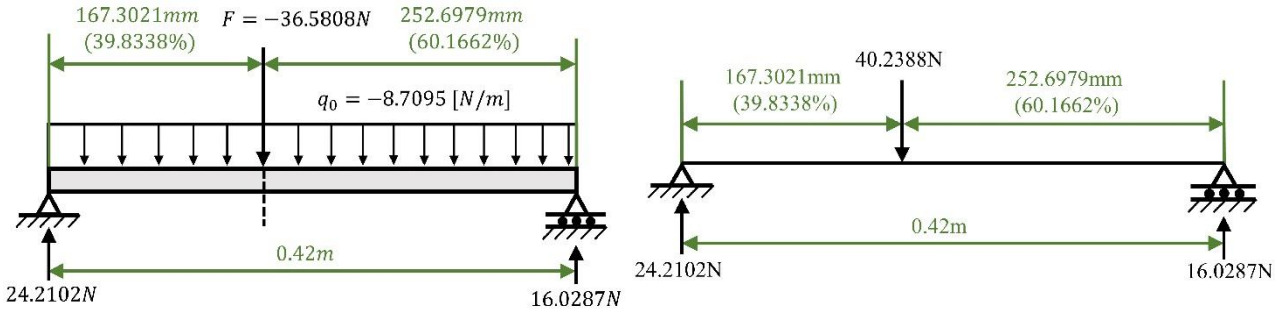

Figure 3 – Analytic models: static (left) and dynamic (right).

The numerical model used for the code verification is shown on Fig.4, it being as similar as possible to all analytic models. As stated before, there are two elements between the disk, each mesh refinement implies the division elements in half, doubling the number of elements, from 2 elements (first grid) to 32 elements (fifth grid).

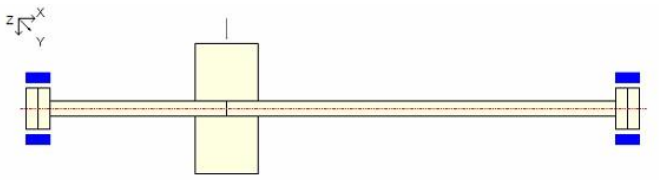

Figure 4 – Numeric model for code verification.

Verification results

All the verification assessments encompass: a rotor with rigid bearings, just the hydrodynamic bearings, and a rotor with short hydrodynamic bearings. The rotors with rigid bearings and oil film bearing models are assessed as verified by the third and fifth mesh respectively. For these three assessments, the verification parameters (from code and calculation verifications) were obtained. Moreover, only the last assessment is presented since it is a combination of the others, and it considered the results of a non-central disk rotor.

The SRQs analyzed are the deflection (displacement and rotation) of the center of the disk (plus bearing clearance) and norms of the unbalance response functions (URFs) from the dynamic model, which is: the disk URF norms of translation and rotation, both bearings URF norms of translation (considering the horizontal, vertical, and combined by hypotenuse URFs). Thus, fourteen SRQs in total are assessed. The calculation of such norms is shown in Eq.19, b is the number of points of amplitudes and Am_i are the amplitude values, the resulting value is always positive.

$$N = \sqrt{\frac{1}{b}\sum_{i=1}^{b} Am_i^2} \tag{19}$$

The observed and theoretical orders of accuracy are shown in Fig. 5. Most of the theoretical order of accuracy of all SRQs tends to approximately 5, which refers only to numerical data, and all observed order of accuracy tends to zero since the numerical SRQs tends to a value slightly different from the analytic SRQs. As mentioned before, since the theoretical order of accuracy is calculated using three successive grids, there will be only three iterations, while the observed order of accuracy is calculated using two successive grids, so there will be four iterations. Nonetheless, the verification results point out the convergence of numerical data, SRQs estimations, error estimations and GCI bands from calculation verification.

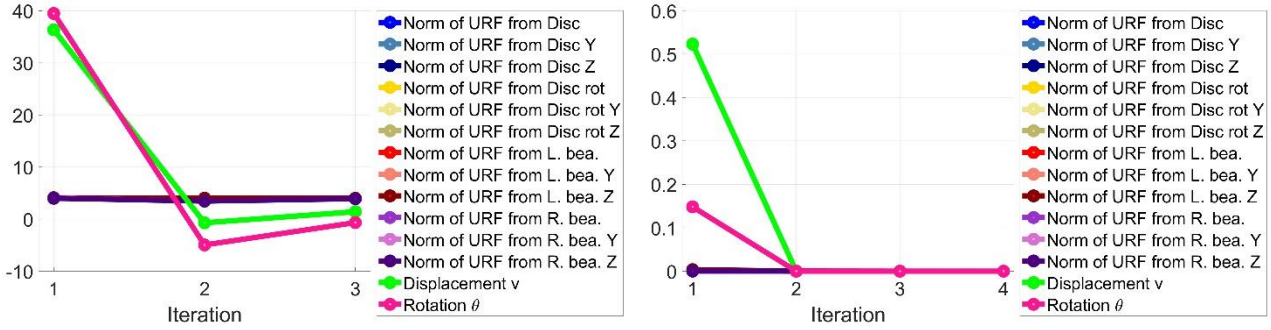

Figure 5 – Theoretical orders of accuracy (left) and observed orders of accuracy (right).

Fig. 6 shows all estimated SRQs, the blue and yellow graphs are the respectively the norms of unbalance response functions of translation and rotation from the disk; the red and purple ones are respectively related to the shaft translations on the left and right bearings; and the green and magenta graphs are respectively the displacement ($[m]$) and rotation ($[rad]$) of the shaft on the center of the disk from the statical analysis.

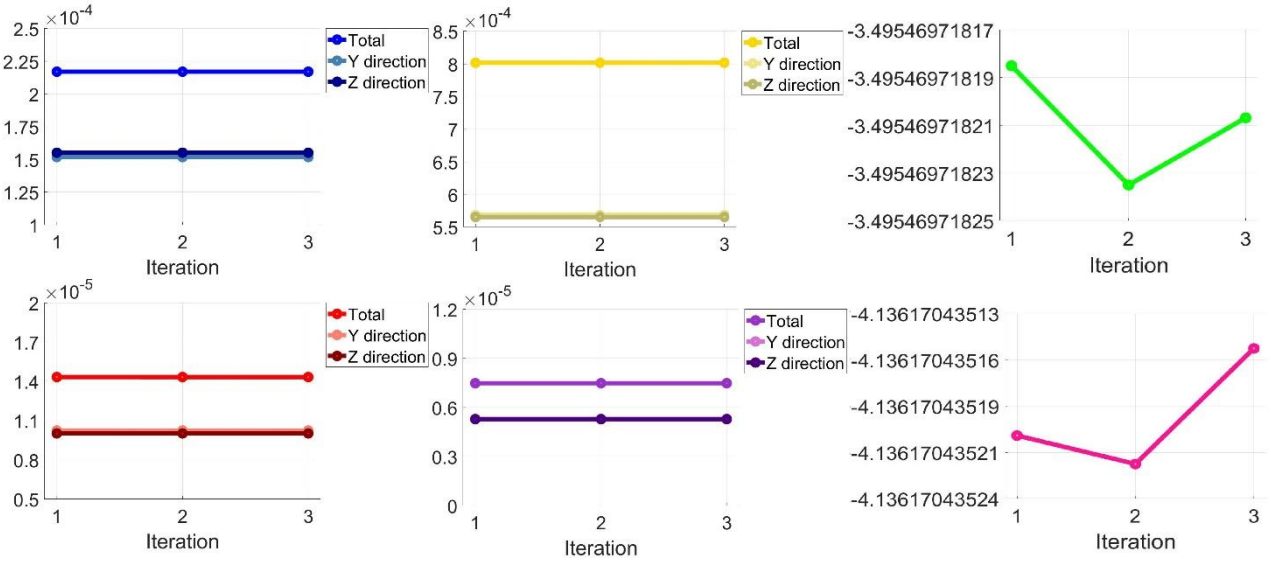

Figure 6 – SRQ estimations of six groups of SRQs from a rotor with non-central disk: dynamic SRQs (four graphs on the left) and static SRQs (two graphs on the right).

The estimated norms on the left are nondimensional but they are based on meters (blue, red and purple graphs) and radians (yellow graphs). A good sign of the software precision is the few changes in all SRQs estimations. As can be observed, the SRQs estimated from the dynamic behavior are on straight lines and the graphs from the static behavior are on very small scale. All the estimated errors for each SRQ are in Fig. 7, which all errors considering all iterations has a value between 10^{-3} to 10^{-6}. This proves that the estimated SRQs are close to the calculated ones.

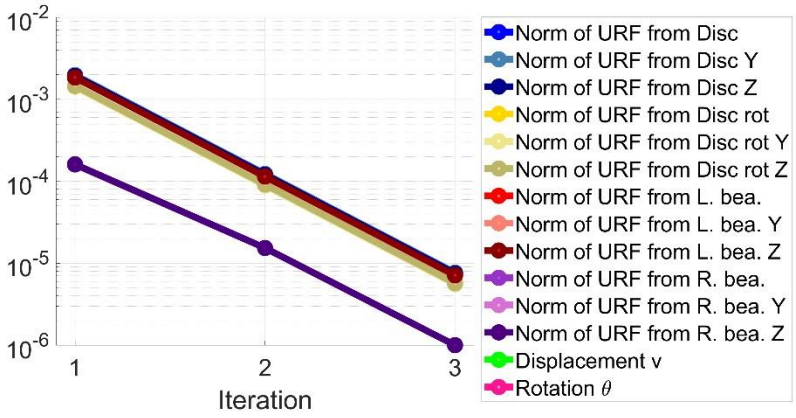

Figure 7 – Error estimations for the rotor SRQs.

And finally, the GCI results are showed in Fig. 8, which are already satisfactory from the first iteration. The highest ones are about 2.5×10^{-5} and satisfy the verification requirement, which is 0.2% ($0.2\% = 0.002 = 2 \times 10^{-3} > 2.5 \times 10^{-5}$). So, the numerical model can be considered verified by the third mesh, which is the finest mesh of the first iteration.

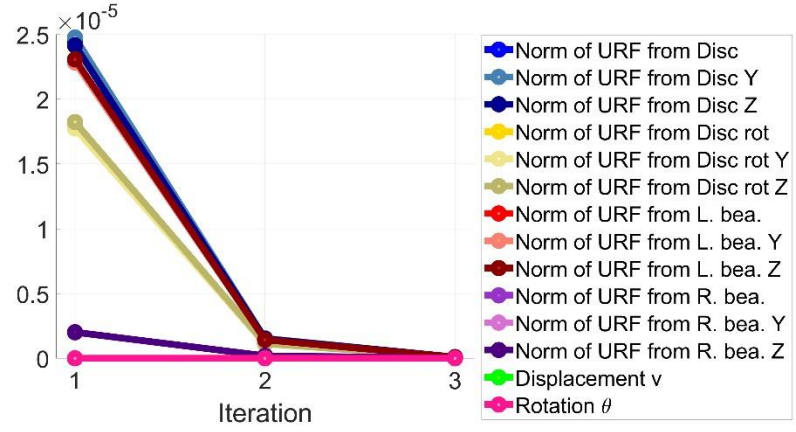

Figure 8 – Grid convergence index of fourteen SRQs of a rotor with non-central disk.

Validation results

The following experimental SRQs from a test rig rotor already shown in Fig. 2 were obtained: total, horizontal and vertical URFs (translations) norms from disk and two bearing regions, at each side of the rotor (nine URFs in total). Again, the total URF is obtained by calculating the hypotenuse of horizontal and vertical directions, then the respective norm can be calculated.

By modeling the same rotor shown in Fig. 2 using the FEM, the respective computational data is obtained. Fig. 9 displays a schematic of the rotor created by the software and used for this assessment, as well as the displacement response at the right bearing. Both URFs (experimental and numerical) must match in order to the numerical model be calibrated as well as possible. Adjustments to the number and size of elements and proportional damping (which is $\beta = 3.5 \times 10^{-5}$ and used for all the verification and validation assessments) are performed for this task. Once the numerical model is calibrated, the validation approach can be executed. In this case, the verified oil film mesh is used.

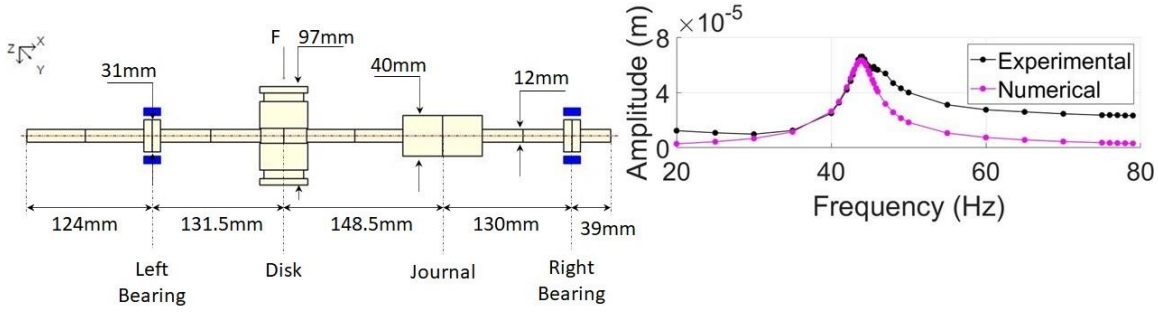

Figure 9 – Schematic rotor with dimensions (left) and numeric - experimental unbalance response function in right bearing (right).

The validation approach considers one set of experimental data which are nine URF norms. Recalling the validation metric in Eq. 18, one must specify the half-width for each SRQ in order to create a probability density function (PDF) and, consequently a cumulative density function (CDF), considering the own SRQ as the mean. With this data and using the Principle of Maximum Entropy, the PDFs can be made, from which the standard deviation is calculated, along with other required parameters of the principle. The summarized input data is shown in Tab. 1.

Table 1 – Experimental and Computational mean values and half-widths of PDFs to be estimated.

URF norms	Experimental mean value of PDF	Computational mean value of PDF	Experimental half-width of PDF	Computational half-width of PDF
Disk	$\boldsymbol{N = 4.6354 \times 10^{-4}}$	$\boldsymbol{N = 4.8660 \times 10^{-4}}$	$\boldsymbol{\Delta = 4.5 \times 10^{-5}}$	$\boldsymbol{\Delta = 2.25 \times 10^{-5}}$
Disk (H. dir.)	$N = 3.5820 \times 10^{-4}$	$N = 3.3986 \times 10^{-4}$	$\Delta = 3.5 \times 10^{-5}$	$\Delta = 1.75 \times 10^{-6}$
Disk (V. dir.)	$N = 2.9421 \times 10^{-4}$	$N = 3.4824 \times 10^{-4}$	$\Delta = 2.8 \times 10^{-5}$	$\Delta = 1.4 \times 10^{-6}$
Left b.	$\boldsymbol{N = 4.4964 \times 10^{-5}}$	$\boldsymbol{N = 3.8912 \times 10^{-5}}$	$\boldsymbol{\Delta = 6.8 \times 10^{-6}}$	$\boldsymbol{\Delta = 3.4 \times 10^{-6}}$
Left b. (H. dir.)	$N = 3.0121 \times 10^{-5}$	$N = 2.7823 \times 10^{-5}$	$\Delta = 4.5 \times 10^{-6}$	$\Delta = 2.25 \times 10^{-6}$
Left b. (V. dir.)	$N = 3.3383 \times 10^{-5}$	$N = 2.7203 \times 10^{-5}$	$\Delta = 5 \times 10^{-6}$	$\Delta = 2.5 \times 10^{-6}$
Right b.	$\boldsymbol{N = 2.6580 \times 10^{-5}}$	$\boldsymbol{N = 2.6501 \times 10^{-5}}$	$\boldsymbol{\Delta = 1.5 \times 10^{-6}}$	$\boldsymbol{\Delta = 7.5 \times 10^{-7}}$
Right b. (H. dir.)	$N = 1.8754 \times 10^{-5}$	$N = 1.8833 \times 10^{-5}$	$\Delta = 1 \times 10^{-6}$	$\Delta = 5 \times 10^{-7}$
Right b. (V. dir.)	$N = 1.8836 \times 10^{-5}$	$N = 1.8645 \times 10^{-5}$	$\Delta = 1 \times 10^{-6}$	$\Delta = 5 \times 10^{-7}$

The probability functions used are two: the gaussian and lognormal. Both have advantages and disadvantages. The Gaussian function was considered because it is easier to master, they are also within the norm and the statistical moment of standard deviation does not significantly exceed the PDF for negative numbers. That is, the resulting PDF will be, in practical terms, zero for negative numbers in the domain, which is important because the norm values are positive. The lognormal function was considered because it is mathematically more adequate, since the domain is from zero to infinity.

Tab. 3. shows all the metrics from the verification approach. The first two columns refer to the horizontal and vertical direction of the left bearing; the third and fourth columns the metrics refer to the disk, and the last two columns refer to the right bearing. It can be stated that the model can represent accurately the horizontal displacement of the rotor, since the SRQs satisfy the validation metric (colored green for number lower than 10%). Regarding the vertical direction, it is only satisfied for the right bearing. The discrepancies found can be related to the proximity of those elements to the motor coupling, which has its own unbalance excitement and misalignment, which is not considered on the numerical model.

Table 3 – All validation approaches metrics.

$\boldsymbol{M^{SRQ}}$	L. Bearing (H)	L. Bearing (V)	Disk (H)	Disk (V)	R. Bearing (H)	R. Bearing (V)
1st V app. (gaussian)	7.63%	18.51%	5.12%	18.36%	0.42%	1.01%
1st V app. (lognormal)	7.63%	18.51%	5.12%	18.36%	0.42%	1.01%

CONCLUSIONS

On the verification of the rotor with hydrodynamic bearings, the first interaction (which considers the first three meshes of the rotor shaft) gives a good result of GCI, which means that the numeric model of finite beam elements and rigid disk element is verified on the third mesh, while the model for the oil film from the bearing is verified at the fifth mesh. It is also possible to observe from Table 3 that most of the validation results are in the expected range of 10% defined initially, except for the left bearing results. Since this bearing lies near the motor coupling, it is more prone to misalignment than the other components, and since the mathematical model used does not consider the effect of misalignment, the presented errors are somewhat expected. Nonetheless, the achieved results can be considered satisfactory.

ACKNOWLEDGMENTS

The authors thank FAPESP #2019/00974-1 and CNPq #307941/2019-1 for the financial support to this research.

REFERENCES

AIAA, “Guide for Verification and Validation of Computational Fluid Dynamics Simulations”, AIAA G-077-1998, American Institute of Aeronautics and Astronautics, Reston, VA.

ASME, 2006, “Guide for Verification and Validation in Computational Solid Mechanics”, ASME V&V 10, New York, NY.

ASME, 2009, "Standard for Verification and Validation in Computational Fluid Dynamics and Heat Transfer", ASME V&V 20, New York, NY.

ASME, 2012, "An Illustration of the Concepts of Verification and Validation in Computational Solid Mechanics", ASME V&V 10.1, New York, NY.

Athe, P., Jones, C., and Dinh, N., 2021, "Assessment of the Predictive Capability of VERA—CS for CASL Challenge Problems", ASME – J. of Verification, Validation and Uncertainty Quantification, Vol. 6, Issue 2, 021003, 17 p., DOI: https://doi.org/10.1115/1.4050248.

Bodner, J and Kaul, V., 2021, "Framework for In Silico Clinical Trials for Medical Devices Using Concepts From Model Verification, Validation, and Uncertainty Quantification (VVUQ)", ASME 2021 Verification and Validation Symposium. 11 p., DOI: https://doi.org/10.1115/VVS2021-65094.

Helton J.C. and Oberkampf W.L., 2004, "Alternative representations of epistemic uncertainty", Reliability Engineering & System Safety, Volume 85, Issues 1–3. pp. 1-10. DOI: https://doi.org/10.1016/j.ress.2004.03.001.

Hibbeler, R., C., 2011, "Mechanics of Materials", Pearson, 8th edition, New Jersey, USA, 888 p.

Hu, K. T., Carnes, B. and Romero, V., 2016, "Introduction: The 2014 Sandia Verification and Validation Challenge Workshop." ASME – J. of Verification, Validation and Uncertainty Quantification, Vol. 1, Issue 1, 010301, 4 p., DOI: https://doi.org/10.1115/1.4032569.

Hills R. G., Pilch M., Dowding K. J., Red-Horse J., Paez T. L., Babuška I. and Tempone R., 2008, "Validation Challenge Workshop". Computer Methods in Applied Mechanics and Engineering, Vol. 197, Issues 29–32, pp. 2375-2380. DOI: https://doi.org/10.1016/j.cma.2007.10.016

Krämer E., 1993, "Dynamics of Rotors and Foundations", Sringer-Verlag, Berlin and Heidelberg, Germany, 384 p.

Oberkampf W.L. Helton J. C., Joslyn C. A., Wojtkiewicz S. F. and Fersone S., 2004, "Challenge problems: uncertainty in system response given uncertain parameters", Reliability Engineering & System Safety, Vol. 85, Issues 1–3. pp. 11-19. DOI: https://doi.org/10.1016/j.ress.2004.03.002.

Nelson, H. D., 1980, "A Finite Rotating Shaft Element Using Timoshenko Beam Theory", ASME – Journal of Mechanical Design, Vol. 102, No. 4, pp. 793-803.

Nelson, H. D.; McVaugh, J. M., 1976, "The dynamics of rotor-bearing systems using finite elements", ASME – Journal of Engineering for Industry, Vol. 98, No. 2, pp. 593-600.

RESPONSIBILITY NOTICE

The authors are the only responsible for the printed material included in this paper.